Reduced model of active-rectifier-based bi-directional charger for vehicle-to-grid

Le Trung Duc[1], Bao-Huy Nguyen[1], Linh Tran[1], Wilmar Martinez[2] and Thanh Vo-Duy[1,*]

[1] *CTI Laboratory for Electric Vehicles,, School of Electrical and Electronic Engineering, Hanoi University of Science and Technology, Vietnam*
[2] *KU Leuven, EnergyVille, Belgium*
[*] *Corresponding author E-mail: thanh.voduy@hust.edu.vn*
DOI: https://doi.org/10.64032/mca.v30i1.372

Abstract

The dramatic increase in the number of electric vehicles (EVs) on the roads may cause a negative impact on the grid, as charging their battery requires a huge amount of power. In such circumstances, Vehicle-to-Grid (V2G) becomes a promising solution that can regulate the energy flow between EVs' batteries and the power system to avoid overloading and enhance power quality. This paper proposes a bi-directional charging control system based on the reduced model of the active rectifier for V2G application. The proposed control system can exchange energy with the grid in V2G mode, limit the charging power in smart charging mode, and control the active and reactive power to the grid. All the controllers of the system are designed based on the average model using energetic macroscopic representation (EMR), hence, they can operate in a wide working range. The performance and functionality of the proposed charger are evaluated by numerically simulating a full charging cycle of the battery with various testing scenarios.

Keywords: *V2G; EMR; Smart Charging*

1. Introduction

The environment and natural resources are becoming an increasingly significant challenge for our modern world. In this context, electric vehicles (EVs) have emerged as a promising solution to mitigate negative environmental impacts and conserve natural resources [1]. EVs operate more efficiently than traditional internal combustion engine (ICE) vehicles, helping to save energy and reduce resource consumption. Furthermore, advancements in battery technology and charging infrastructure are making important progress, enhancing driving range, reducing charging times, and making it more convenient to use in daily life. Using EVs is a crucial step towards building a more sustainable, cleaner, and modern future.

The large-scale deployment of EV charging infrastructure poses significant challenges for the existing power grid. One major concern is voltage variation. When a large number of EVs are charged simultaneously in a localized area, the sudden increase in load demand can lead to voltage drops or fluctuations. This can adversely affect the performance of both EV chargers and household appliances. Additionally, grid frequency stability may also be compromised. The irregular and unpredictable nature of EV charging loads, particularly during peak hours, can create an imbalance between supply and demand, resulting in deviations in system frequency and potentially leading to grid instability. Moreover, fast EV charging can degrade power quality by introducing harmonics, causing voltage flicker, and resulting in a low power factor.

Therefore, there is an urgent need for a charging infrastructure that is efficient, scalable, safe, and sustainable to ensure the stable operation of future power systems. For that, in addition to providing energy to EVs, charging stations must also maintain grid stability. Numerous studies have been conducted to improve EV charging technology, focusing on various aspects.

In the first aspect, research on charging station design aims to develop optimal charging architectures that enhance energy transfer efficiency and integration with the electrical system. Investigations in this area focus on improving energy converters, particularly DC-AC and DC-DC converters, to minimize energy losses and enhance grid compatibility [3–5]. The studies presented in [6] and [7] offer in-depth insights into circuit configurations for both AC-DC and DC-DC conversion stages. Popular topologies under investigation include multi-level inverters, resonant converters, and high-frequency converters, all designed to optimize the size and performance of charging stations. Additionally, Wireless Power Transfer (WPT) technology is also being explored to enhance the convenience and safety of the EV charging process [8, 9].

Studies on control strategies for optimizing charging performance have been implemented to reduce energy losses and maintain system stability [10–14]. Control methods applied include hysteresis control, PI/PID control, and LQR control [15]. Notably, advanced control algorithms based on artificial intelligence (AI) are being investigated to automatically adjust charging currents, thereby improving performance and protecting the electrical system from undesirable fluctuations [16].

Research works aimed at optimizing the charging process to ensure battery longevity and usage efficiency have proposed various charging profiles, among which the most common are the Constant Current (CC), Constant Voltage (CV), and hybrid CC/CV modes [17–19]. These studies also focus on reducing battery operating temperatures and limiting the maximum state of charge to decelerate battery degradation [20, 21].

Currently, research on Vehicle-to-Grid (V2G) technology

Received: 10 September 2025; Revised: 03 December 2025; Accepted: 18 December 2025.

is being conducted to enable EVs not only to consume but also to supply electricity back to the grid, thus aiding in load balancing, supporting the integration of renewable energy, and optimizing energy management. However, current V2G studies primarily focus on energy management aspects, considering the charging station as an ideal connection point that can be fully controlled, rather than concentrating on power electronics control.

EV charging is a specific topic within the broader research field of power electronics, which focuses primarily on the design, modeling, and control of power converters. Researchers in this field conduct detailed investigations into switching behavior, operational modes, and various converter topologies. Such studies often require precise observation of voltage and current waveforms at very high time resolution, typically in nanoseconds, to capture the rapid switching events in semiconductor devices, which significantly increases the computational load. As a result, even simulating a few seconds of converter operation can require significant processing power and memory resources, particularly when detailed models of power semiconductor devices and control loops are included. Additionally, when these converters are integrated into larger systems, such as EV charging stations or grid-connected charging networks, the complexity of the overall simulation increases exponentially. Consequently, long-term or real-time simulations of EV charging systems at the power electronics level are often impractical. These simulations are highly resource-intensive and frequently exceed the capabilities of standard simulation platforms, leading to a lack of a comprehensive overview of system performance.

In this paper, we propose a design of a charging station that allows bidirectional energy exchange with the grid. The proposed system is first represented by the Energetic Macroscopic Representation (EMR) method. From that, the control scheme is deduced by the Inversion-based Control (IBC) principle. The studied charging station can support the grid by controlling active and reactive power, as well as limiting the charging power as demanded. The paper has the following contributions.

- The proposed charging system can operate in various modes, including conventional charging, smart charging, and V2G mode (bidirectional charging).
- The proposed system enables long-term system simulations. In other words, the system can be observed over a long duration of charging, allowing a thorough evaluation and observation of operational effectiveness and the impact of the charging process on the grid.
- The paper analyses the behavior of the system when changing the charging modes. For that, a controller switching technique is also proposed to smooth the charging process and enhance the control performance.

The proposed charging system is validated by simulation and evaluated with various testing scenarios. The results illustrate the practical feasibility of V2G in real-life applications.

The paper is organized as follows. Section II describes the configuration of the charging system. Section III proposes the control and management system design. Section IV validates the proposed system and presents the simulation results of the charging system. Finally, conclusions are given in Section V.

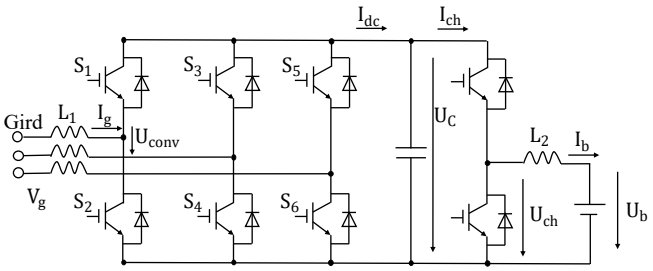

Figure 1: System Configuration.

2. System configuration and modeling

This paper employs the EMR method to represent the system and design the charging control scheme using the averaged model instead of the switching model. Consequently, the system can be simulated over an extended period, thereby supporting the application of bidirectional V2G.

EMR is a graphical representation method, is almost immediately applied in the research of systems with various interacting physical components, such as wind power systems [24], electrochemical processes [25], and notably in energy exchange systems within electric vehicles. There are principles of the EMR that must be followed during model development.

- Interaction principle: Elements in the system are bidirectionally linked based on the principles of action and reaction.
- Causality principle: Causality integration is employed in the method, manifested in the accumulation element describing the time-dependent relationship between variables.
- Inversion principle: To attain the desired input value from the desired output, the control structure of the system is regarded as an inverted model for each element.

2.1 System configuration

Fig. 1 illustrates a commonly used charging system configuration. The grid is connected to the input AC inductors L_1 for filtering, then passes through an active rectifier stage to create a DC voltage at the capacitor. At this point, this voltage is controlled to achieve a set value. The voltage at the capacitor goes through a DC/DC stage and is connected to a DC inductor L_2 and the vehicle battery. The current through the inductor coil L_2 and the voltage of the battery are controlled sequentially in CC and CV charging modes.

2.2 System modeling

The system model components are represented by yellow and green blocks within the System Modules Layer, as illustrated in Fig. 4. The arrows indicate the interaction variables that are exchanged between the modules. The detailed description of each component's model is presented below.

- Grid: The power grid comprises three line-to-line voltages, each with a peak amplitude of V_g and an angular frequency of ω. These line voltages are phase-shifted by an angle of $\frac{2\pi}{3}$ with respect to one another. The mathematical representation of the grid voltages is as follows:

$$\begin{cases} U_{ga} = V_g sin(\omega t + \frac{2\pi}{3}) \\ U_{gb} = V_g sin(\omega t) \\ U_{gc} = V_g sin(\omega t - \frac{2\pi}{3}) \end{cases} \quad (1)$$

- Grid-side Inductor L_1: The voltage drop across the grid-side inductor (U_{L1}) is calculated as the difference between the grid voltage (U_g) and the converter's input voltage (U_{conv}). In the time domain, this relationship can be represented by the following equation:

$$U_g - U_{conv} = L_1 \frac{dI_g}{dt} + R_1 I_g \quad (2)$$

where L_1 denotes the inductance value of the grid-side inductors, and R_1 represents their resistance.
For the purpose of control system design, the circuit elements are modeled in the frequency domain with the Laplace operator. Consequently, the relationship between the relevant quantities associated with inductor L_1 can be expressed as:

$$I_g(s) = (U_g(s) - U_{conv}(s)) \frac{1}{L_1 s + R_1} \quad (3)$$

- Battery-side Inductor L_2: The voltage drop across this inductor (U_{L2}) is equal to the difference between the output voltage of the chopper (U_{ch}) and the battery voltage (U_b). The corresponding expression can be derived as follows:

$$I_b(s) = (U_{ch}(s) - U_b(s)) \frac{1}{L_2 s + R_2} \quad (4)$$

where, L_2 represents the inductance of the battery-side inductor, and R_2 denotes its resistance.
- DC-link Capacitor: The voltage across the capacitor (U_c) is equal to the integral of the current flowing through it (I_c), divided by its capacitance (C). This relationship can be expressed as:

$$U_c = \frac{1}{C} \int I_c \, dt \quad (5)$$

where, $I_c = I_{dc} - I_{ch}$, and I_{dc} is the output current of the converter, and I_{ch} is the input current of the chopper. By transforming this expression to the frequency domain, the relationship between the capacitor current and voltage can be described as:

$$U_c(s) = (I_{dc}(s) - I_{ch}(s)) \frac{1}{Cs} \quad (6)$$

- Active rectifier: The control signal m_1 consists of three modulation functions in types of sine waves, $m_1 = [m_a, m_b, m_c]^T$

$$\begin{cases} U_{conv} = m_1 \frac{U_c}{2} \\ I_{dc} = m_a I_{ga} + m_b I_{gb} + m_c I_{gc} \end{cases} \quad (7)$$

- The DC/DC converter (chopper):

$$\begin{cases} I_{ch} = m_2 I_{dc} \\ U_{ch} = m_2 U_c \end{cases} \quad (8)$$

where, m_2 is the modulation function of the chopper.

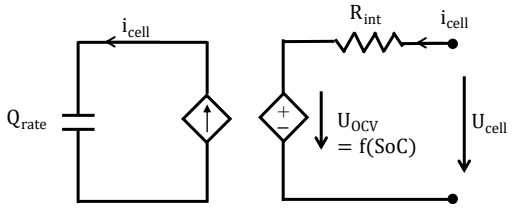

Figure 2: Equivalent circuit of battery cell

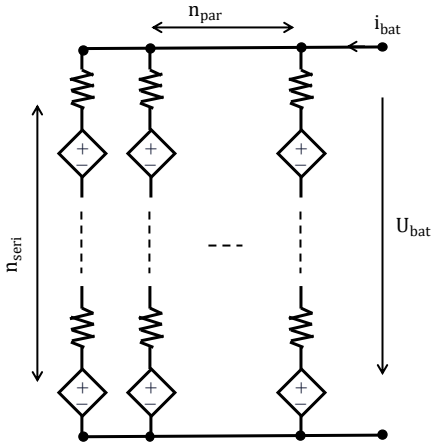

Figure 3: Equivalent circuit of battery pack.

- Vehicle battery: A vehicle battery cell can be represented by an internal resistor R_b which is connected in series with a very high energy-density capacitor with capacitance Q_b as described in Fig. 2. For each cell of the battery pack, the model can be deduced from its equivalent circuit as follows.

$$\begin{cases} SOC = \frac{1}{3600 Q_b} \int I_{cell} \\ U_{cell} = I_{cell} R_b + U_{OCV} \end{cases} \quad (9)$$

where, U_{OCV} is the open circuit voltage of the battery cell which is a function of the state-of-charge (SOC), U_{cell} and I_{cell} denote output voltage and current of each cell, respectively.
In order to design a battery pack, one can generate combinations of cells by connecting them in a given configuration. Let us define n_{seri} number of battery cells that are connected in series and n_{par} number of parallel branches as described in Fig. 3, the power sharing among cells inside the pack can be written:

$$U_b = (\frac{I_b}{n_{par}} R_b + U_{OCV}) n_{seri} \quad (10)$$

3. Proposed control and management system design

Based on the inversion principle of the EMR, the control architecture of the system is designed as illustrated in Fig. 4. The key components are the blue blocks located in the Control Layer, which include the current and voltage controllers, as well as the inverted models of the converter and chopper. The Estimation Layer consists of pink elements that are responsible for estimating the rotational angle of the grid voltage. Meanwhile, the dark blue blocks in the Strategy Layer coordinate the operation of the control scheme, which helps generate the desired power reference.

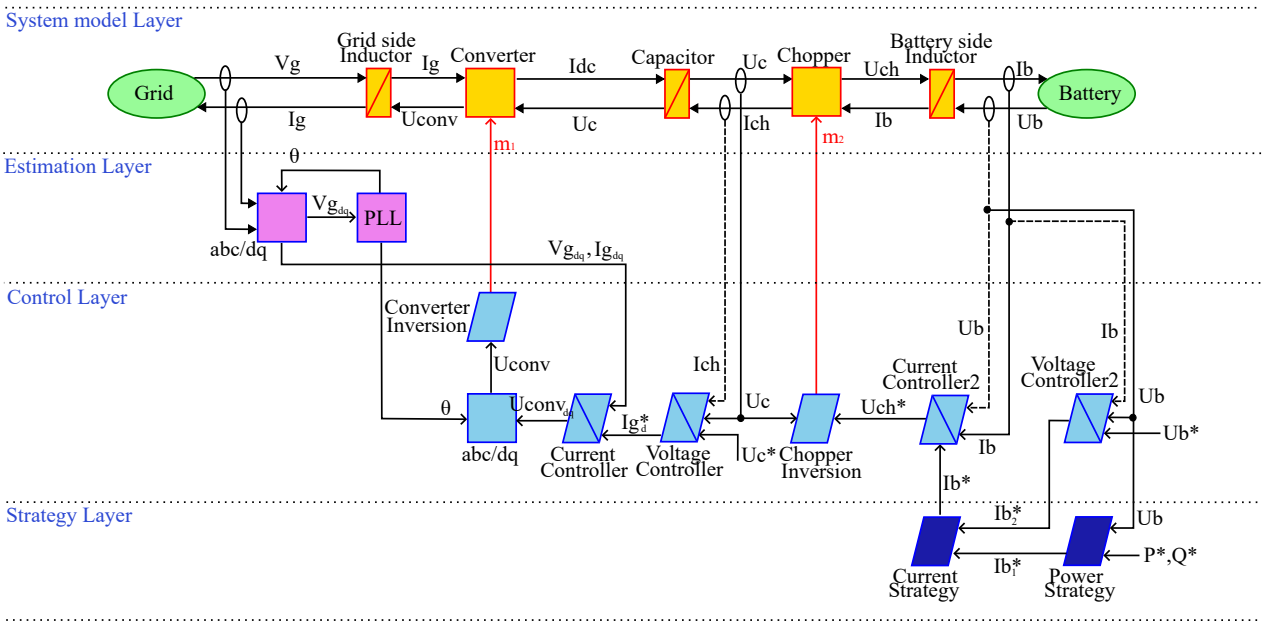

Figure 4: System Representation and Control Scheme.

The control of the system involves two concurrent processes. The first process, i.e., active rectification, aims to maintain a constant voltage level in the DC-link capacitor. The second process focuses on controlling the charging power, where the charging current (I_b) is calculated based on a reference charging power. Furthermore, the State of Charge (SOC) of the battery is used to decide whether to apply Constant Current (CC) or Constant Voltage (CV) charging mode.

Additionally, the control system is designed in the dq coordinate system for some benefits, such as simplification, reduced dimensions, and increased system stability.

3.1 Phase-locked loop

Located in the Estimation Layer, the phase-locked loop (PLL) operates based on controlling the angular velocity of the dq-coordinate axis system such that the projection of the grid voltage vector onto the q-axis is zero (at that time, the grid voltage vector lies along the d-axis). Consequently, the angular velocity of the coordinate system axis tracks the angular velocity of the grid voltage vector. By determining the angular velocity and angle of the coordinate system axis, the frequency and phase angle of the grid voltage can be calculated.
The transfer function of the phase control loop circuit can be described by a second-order system G_{pll}.

$$G_{pll} = \frac{Kp_{pll}s + Ki_{pll}}{s^2 + Kp_{pll}s + Ki_{pll}} \tag{11}$$

By comparing it with a standard second-order function, we have the control parameters of the PLL.

$$\begin{cases} Kp_{pll} = 2\frac{2\pi}{Tres_{pll}}\xi \\ Ki_{pll} = \frac{2\pi}{Tres_{pll}}^2 \end{cases} \tag{12}$$

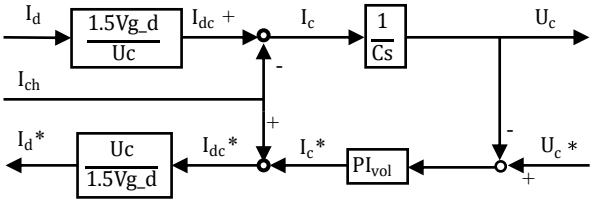

Figure 5: Block diagram of the capacitor voltage control loop.

3.2 System control design

3.2.1 AC/DC control

Aiming to regulate the DC-link capacitor voltage to a constant level, this process consists of 2 main control loops: the capacitor's voltage control loop and the current control loop.

Voltage control loop As illustrated in Fig. 5, the actual value U_c is compared with the reference value U_c^*, then passed through a PI controller to generate the set value I_c^*. Next, disturbances are compensated for by adding the value I_{ch} to create the quantity I_{dc}^*. If losses in the rectifier and in the inductor are neglected, then:

$$\frac{I_{dc}(t)}{I_{gd}(t)} = \frac{\frac{3}{2}V_{gd}}{U_c} \tag{13}$$

The transfer function of the closed-loop system:

$$G_{vol} = \frac{\frac{kp_{vol}}{C}s + \frac{ki_{vol}}{C}}{s^2 + \frac{kp_{vol}}{C}s + \frac{ki_{vol}}{C}} \tag{14}$$

Similar to the control design procedure of the PLL, the voltage controller parameters can be achieved.

$$\begin{cases} kp_{vol} = 2\xi_{vol}\omega_{vol}C \\ ki_{vol} = \omega_{vol}^2 C \end{cases} \tag{15}$$

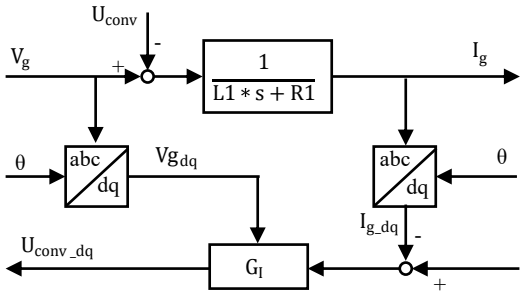

Figure 6: Grid-side Inductor's current control loop.

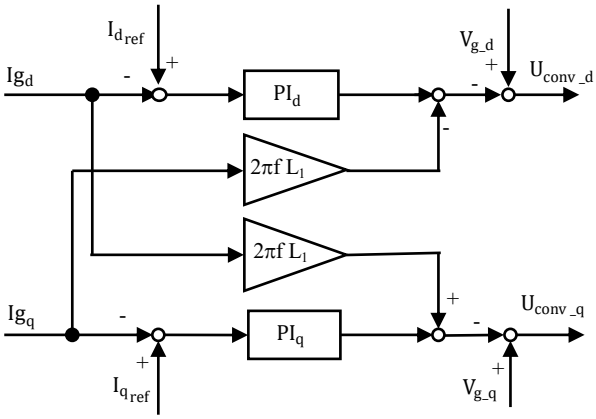

Figure 7: Current control block G_I.

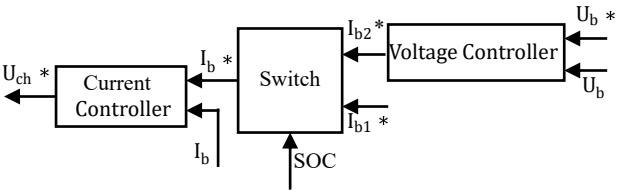

Figure 8: CC, CV Charging Control.

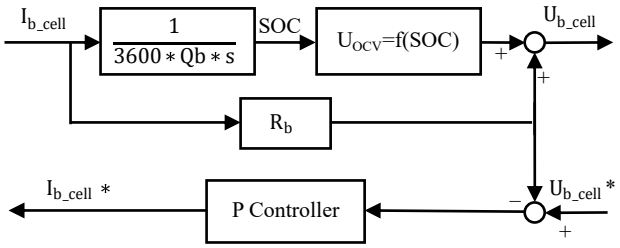

Figure 9: Battery's voltage control loop.

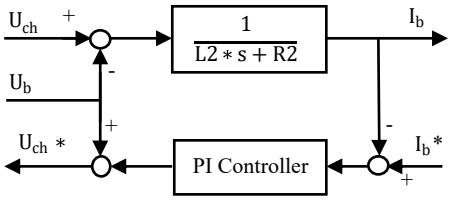

Figure 10: Charging current control loop.

Current control loop (Fig. 6–7) In the abc coordinate system.

$$\begin{cases} U_{ga} = R_1 I_{ga} + L_1 \frac{dI_{ga}}{dt} + U_{conv_a} \\ U_{gb} = R_1 I_{gb} + L_1 \frac{dI_{gb}}{dt} + U_{conv_b} \\ U_{gc} = R_1 I_{gc} + L_1 \frac{dI_{gc}}{dt} + U_{conv_c} \end{cases} \tag{16}$$

Using Park transformation, the voltage equation in the dq-frame can be obtained as follows..

$$\begin{cases} U_{conv_d} = U_{gd} - (R_1 I_{gd} + L_1 \frac{dI_{gd}}{dt}) + \omega L_1 I_{gq} \\ U_{conv_q} = U_{gq} - (R_1 I_{gd} + L_1 \frac{dI_{gd}}{dt}) - \omega L_1 I_{gd} \end{cases} \tag{17}$$

From that, we have the parameters of the current controllers.

$$\begin{cases} ki_{cur} = \frac{ln(20)}{Tres_{cur}} R_1 \\ kp_{cur} = Ki_{cur} \frac{L_1}{R_1} \end{cases} \tag{18}$$

3.2.2 DC/DC control

The goal of this process is to maintain a constant current flowing through the vehicle's battery in CC charging mode and reduce that current in CV charging mode.

The system comprises two main control loops: the battery's voltage control loop and the charging current control loop. When the State of Charge (SOC) of the battery is less than 80%, the current controller directly takes the set current value without obtaining it from the output of the battery voltage controller. When $SOC \geq 80\%$, the set current value is taken from the battery voltage controller.

Battery's voltage control loop (Fig. 9) The battery can be seen as a big capacitor, hence its model is an integrator. For that, a proportional controller is utilized to regulate the battery voltage. The control parameter is given as in (19).

$$kp_{volbat} = \frac{ln(20)}{Tres_{volbat}} 3600 Q_b \tag{19}$$

Charging current control loop (Fig. 10) Using the settling-time assignment method for a first-order inertial object, the parameters of the charging current controller can be determined as follows.

$$\begin{cases} ki_{curbat} = \frac{ln(20)}{Tres_{curbat}} R_2 \\ kp_{curbat} = Ki_{curbat} \frac{L_2}{R_2} \end{cases} \tag{20}$$

3.3 Charging and discharging strategy

The objective of this section is to select and calculate the charging current I_b^* based on the current I_{b1}^* (output of the Power Charging Strategy unit) and the current I_{b2}^* (output of the Voltage Controller 2 unit).

The current I_{b1}^* is calculated by taking the permissible charging or discharging power (P_{ref}) and dividing it by the current voltage of the vehicle's battery (U_b). It is then constrained by the maximum charging current the battery can handle (I_{bmax}) and the maximum discharging current the battery can handle (I_{bmin}). Different types of electric vehicle batteries have different I_{bmax} and I_{bmin} values depending on the design and regulations of each specific battery type, as well as the battery charging system used. This is done to ensure the safety and longevity of the battery.

In discharge mode ($P_{ref} < 0$), the current I_b^* is taken from I_{b1}^* since there is no need to follow the CC/CV charging mode. When $SOC < 20\%$, the discharging is stopped to ensure the durability of the vehicle's battery, and the value of 20% can be replaced by other values depending on the battery type and charging station.

Table 1: Parameters of Model

Grid voltage	$V_g = 380V$
Grid frequency	$f = 50Hz$
Inductor	$L_1 = 10mH, R_1 = 0.005\Omega$ $L_2 = 4.7mH, R_2 = 0.005\Omega$
Capacitor	$C = 5.6mF$
Battery	$n_{par} = 22; n_{seri} = 88$ $U_{rate} = 3.6V; Q_{rate} = 3.3Ah$
Phase-locked loop	$kp_{pll} = 25.3$ $ki_{pll} = 157.91$
U_c **controller**	$U_{c-ref} = 800V$ $kp_{vol} = 0.7$ $ki_{vol} = 22.1$
Current controller	$kp_{cur} = 1.5$ $ki_{cur} = 3$
Battery voltage controller	$kp_{volbat} = 32.7$
I_b **control loop**	$kp_{curbat} = 1.3$ $ki_{curbat} = 1.4$

On the other hand, in charging mode ($P_{ref} \geq 0$), when $SOC \geq 80\%$: $I_b^* = I_{b2}^*$. And the current I_{b2}^* is always limited by I_{b1}^* to keep the charging power within the allowed limits. The charging current I_b^* is taken from I_{b1}^* when $SOC < 80\%$

4. Results

4.1 Testing scenarios

The charging system is simulated under three representative scenarios as follows.

Scenario 1: Charging without power limitation: During times of low grid demand, the charger allows the vehicle to charge at its maximum power capacity. The vehicle is charged using CC and CV modes, with no requirement to push energy back into the grid.

Scenario 2: Charging with Limited Power: During peak hours, charging stations implement a power limit, resulting in a lower charging current for vehicles. This can be seen as the smart charging mode or unidirectional V2G.

Scenario 3: Integrating Charging and Discharging: At times, the electrical grid may need to draw energy from electric vehicles to maintain balance. In this scenario, electric vehicles are charged and discharged regularly to test the stability of the system. In practice, the occurrence of pushing energy back into the grid may happen less frequently.

The simulation parameters of the studied system are listed in Table 1.

4.2 Model validation

It is important to consider the accuracy of the developed system model. To do this, a model using elements from the Simscape library in Matlab/Simulink is employed to compare the results with those of the average model based on the EMR method. The system model, based on physical elements in the Simscape library (switching model), is built according to the configuration shown in Fig. 1, while the identical control system is used for both the EMR and switching models. Since

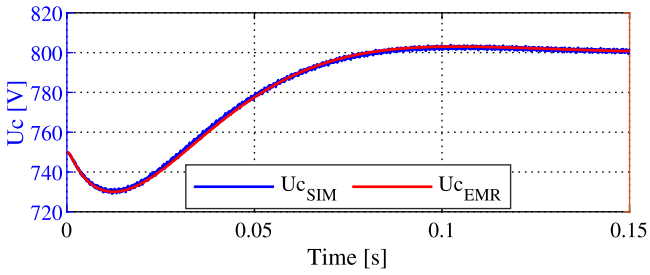

Figure 11: Capacitor voltage U_c in both models

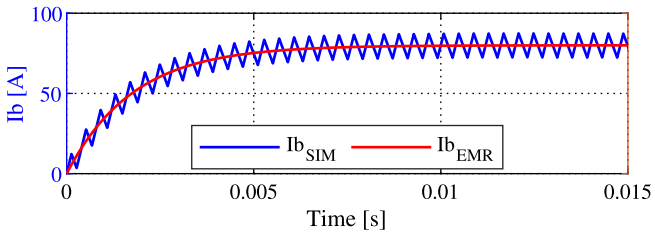

Figure 12: Current I_b in both models over a short period of time.

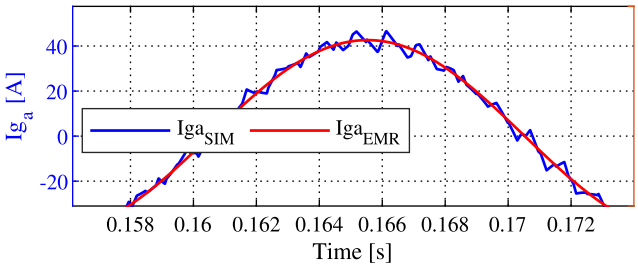

Figure 13: Grid current in phase a (I_{ga}) over a short period of time.

only short-term comparisons can be made due to the switching behavior of the Simscape element, the electric vehicle battery is treated as a voltage source.

As illustrated in Fig. 11–13, the results obtained from both models are similar, with only minor differences caused by the switching phenomenon. From this comparison, the system model using the EMR method is validated and can be used for further testing scenarios.

4.3 Numerical result

Scenario 1: Charging Without Power Limitation results are illustrated in Fig. 14–17. In this scenario, the vehicle is charged in CC mode when the battery SOC is less than 80%. During this phase, the charging utilizes the maximum permissible battery current (I_{bmax}).

Once the SOC reaches 80% and transitions to CV mode, the charging current gradually decreases to 0 A. Concurrently, the battery voltage (U_b) increases steadily until it reaches its maximum value (U_b^*).

The simulation of the charging process is performed from a SOC of 20% to 100%. The results is presented in Fig. 14–16.

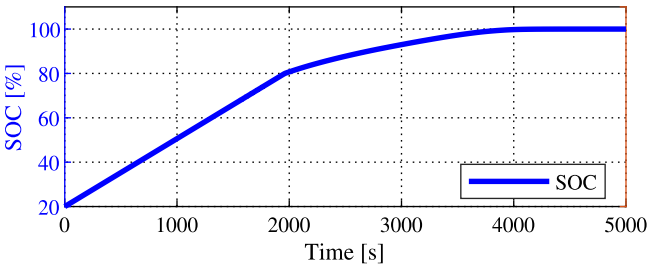

Figure 14: SOC of the battery during the charging process.

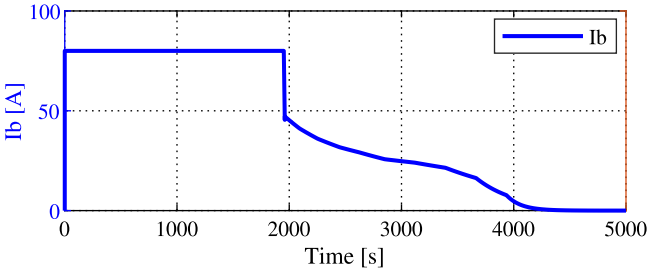

Figure 15: Charging current of the battery.

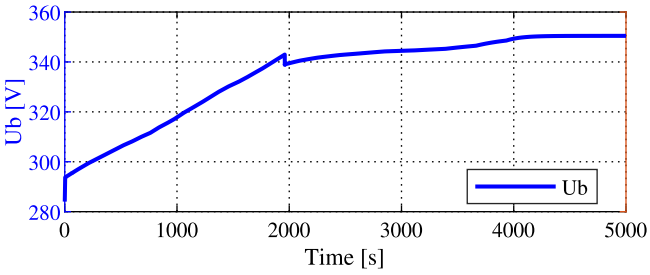

Figure 16: Voltage of the battery during the charging process.

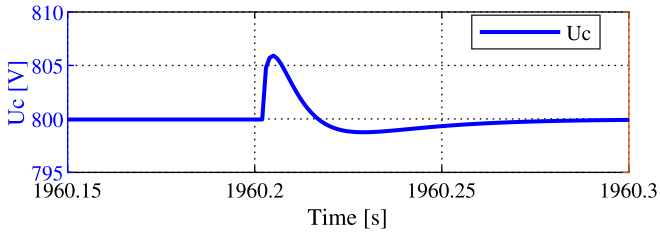

Figure 17: Capacitor voltage C when switching charging modes. (The capacitor voltage U_c is maintained at $800V$ throughout the charging process. At the moment of switching the charging mode, U_c experiences fluctuations due to the sudden change in current I_b.)

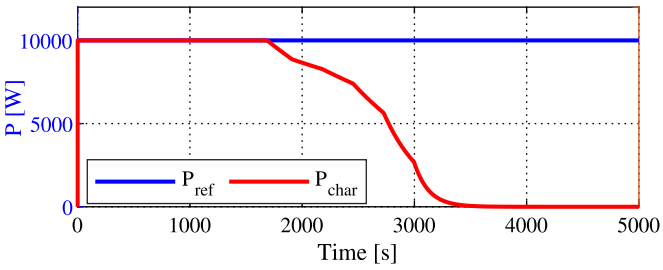

Figure 18: Permissible charging power and actual charging power.

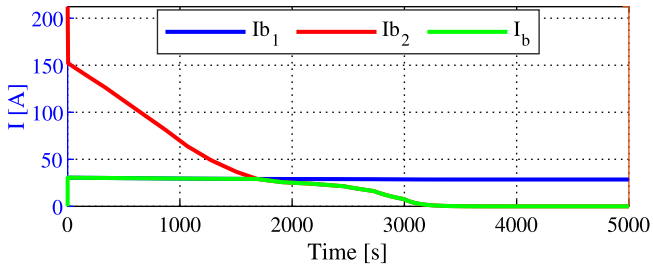

Figure 19: Permissible charging current and actual charging current.

During the CC phase of charging, the SOC increases rapidly, while the increase is slower during the CV phase. The SOC rises from 20% to 80% in approximately 30 minutes, which meets the requirements for a fast-charging system. However, it takes an additional 30 minutes or more for the battery to reach a full charge.

Scenario 2: The results of Charging the vehicle with limited power test are described in Fig. 18–19. In this scenario, we assume that the maximum permissible power of the charging station (P_{ref}) is 10kW. The system is simulated with SOC starting at 70%

In Fig. 19, as discussed in the control system design, when SOC is less than 80%, the current I_{b1}^* (represented by the blue line) gradually decreases as the voltage U_b increases ($I_{b1}^* = \frac{P_{ref}}{U_b}$).

When SOC reaches to the value of 80% or higher, the current controller is set to a value of I_{b2} (indicated by the red line). However, I_{b2} is still limited by I_{b1}. As a result, the charging current I_b (the yellow line) continues to follow its previous trend until I_{b2} becomes smaller than I_{b1}. At that point, the charging current decreases significantly.

Scenario 3: Integrating charging and discharging: Test results are depicted in Fig. 20–22. As shown in Fig. 20, the reference charging power value varies continuously, with transitions between charging and discharging modes. The blue curve represents the permissible charging power of the charging station, which takes on negative values during discharging mode. Meanwhile, the red curve indicates the actual response of the charging power. When the vehicle's allowable charging power range is considered, the two curves align perfectly. However, there are moments when the curves diverge because the permissible charging power of the station exceeds the vehicle battery's allowable limits, which are determined by the vehicle's specific design. From the actual charging power response of the station, the charging current can be determined, as illustrated in Fig. 21. Furthermore, the current and voltage of phase A are examined during the transitions between charging and discharging modes, as illustrated in Fig. 22.

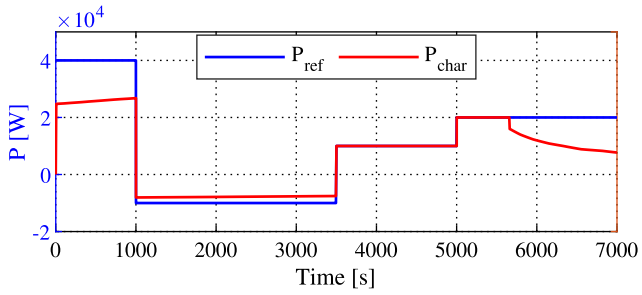

Figure 20: Permissible charging power and actual charging power.

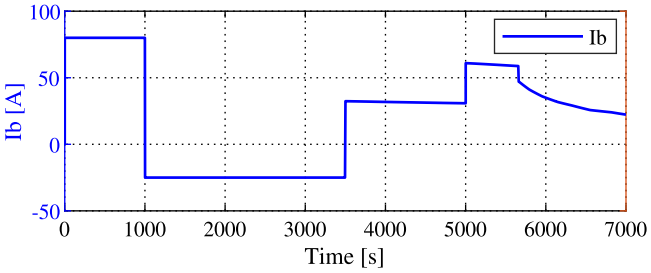

Figure 21: Battery current I_b.

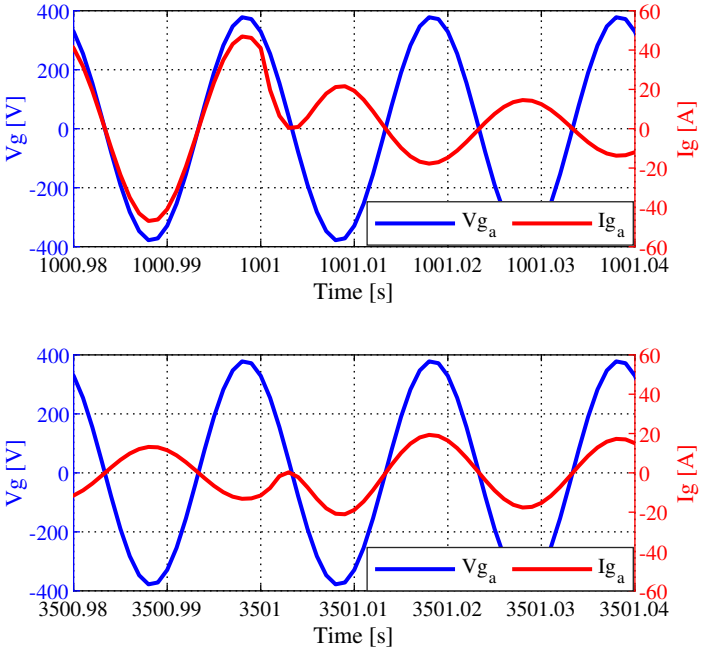

Figure 22: Comparison the phase of V_{ga} and I_{ga}. When switching from charging and discharging modes, V_g and I_g transition from in-phase to out-of-phase. Conversely, when switching from discharging to charging the battery, V_g and I_g transition from out-of-phase to in-phase. From the obtained values, it can be seen that the system remains stable when continuously changing the value of P_{ref}.

5. Conclusion

The paper has studied the V2G Bidirectional charging system, its optimization compared to other current charging methods. The project has also explored the EMR method, built and modeled the V2G Bidirectional charging system using the EMR method, designed and calculated current control systems and voltage control systems. The charging system is simulated using an average model based on the EMR method and a Simscape model in MATLAB Simulink software. The two models that yield similar results have demonstrated the precision of the EMR method. The charging system can respond to real-time power demand, enabling the calculation of the charging current supplied to the battery under the CC-CV charging method.

This research provides a theoretical foundation for the development of smart chargers in V2G systems. By demonstrating the effectiveness of the EMR approach, it simplifies the modeling and control process while offering a basis for large-scale practical deployment of V2G charging stations. Additionally, the results can enhance renewable energy integration, improve grid stability, and support the advancement of sustainable green transportation.

Future studies can be expanded into areas such as optimizing charger efficiency, improving the dynamic response under rapidly changing load conditions, conducting experimental validations, and integrating intelligent energy management solutions. These directions will contribute to the realization of a more practical V2G system.

Funding - This research is funded by Hanoi University of Science and Technology (HUST) under project number T2023-TD-006

References

[1] F. Naseri, E. Farjah, and T. Ghanbari, “An efficient regenerative braking system based on battery/supercapacitor for electric, hybrid and plug-in hybrid electric vehicles with BLDC motor,” IEEE Trans. Veh. Technol., vol. 66, no. 5, pp. 3724–3738, May 2017.

[2] C. McKerracher et al., "Electric vehicle outlook 2021," BloombergNEF, London, U.K., Tech. Rep., Aug. 2021.

[3] Abdelfatah Ali, Hossam H. H. Mousa, Mostafa F. Shaaban, Maher A. Azzouz, and Ahmed S. A. Awad, “A Comprehensive Review on Charging Topologies and Power Electronic Converter Solutions for Electric Vehicles," 2024.

[4] XU-FENG CHENG, CHENYANG LIU, DIANLONG WANG, AND YONG ZHANG “State-of-the-Art Review on Soft-Switching Technologies for Non-Isolated," 2021.

[5] Michael Antivachis, Jon Azurza Anderson, Dominik Bortis, and Johann Walter Kolar, “Analysis of a Synergetically Controlled Two-Stage Three-Phase DC/AC Buck-Boost Converter," 2020

[6] M. Yilmaz and P. T. Krein, "Review of battery charger topologies, charging power levels, and infrastructure for plug-in electric and hybrid vehicles," IEEE Trans. Power Electron., vol. 28, no. 5, pp. 2151–2169, May 2013.

[7] H. Ramakrishnan and J. Rangaraju, "Power topology considerations for electric vehicle stations," Texas Instrum. Appl. Rep., Texas Instrum., Dallas, TX, USA, Tech. Rep. SLLA497, Sep. 2020.

[8] S. Liu, Z. Ye, and W. Lu, "Electric vehicle dynamic wireless charging technology based on multi-parallel primary coils," in Proc. IEEE Int. Conf. Electron. Commun. Eng. (ICECE), Dec. 2018, pp. 120–124.

[9] C.-G. Kim, D.-H. Seo, J.-S. You, J.-H. Park, and B. H. Cho, "Design of a contactless battery charger for cellular phone," IEEE Trans. Ind. Electron., vol. 48, no. 6, pp. 1238–1247, Dec. 2001.

[10] M.-C. Ancuti, C. Sorandaru, S. Musuroi, and V.-N. Olarescu, "High efficiency three-phase interleaved buck-type PFC rectifier concepts," in Proc. 41st Annu. Conf. IEEE Ind. Electron. Soc. (IECON), Nov. 2015, pp. 7763–7768.

[11] T. B. Soeiro, T. Friedli, and J. W. Kolar, "Swiss rectifier—A novel three-phase buck-type PFC topology for electric vehicle battery charging," in Proc. 27th Annu. IEEE Appl. Power Electron. Conf. Expo. (APEC), Feb. 2012, pp. 2617–2624.

[12] T. B. Soeiro, M. L. Heldwein, and J. W. Kolar, "Three-phase modular multilevel current source rectifiers for electric vehicle battery charging systems," in Proc. Brazilian Power Electron. Conf., Oct. 2013, pp. 623–629.

[13] B. Zhang, S. Xie, X. Wang, and J. Xu, "Modulation method and control strategy for full-bridge-based Swiss rectifier to achieve ZVS operation and suppress low-order harmonics of injected current," IEEE Trans. Power Electron., vol. 35, no. 6, pp. 6512–6522, Jun. 2020.
[14] A. U. Rahman, N. Campagna, F. Pellitteri, A. O. Di Tommaso, and R. Miceli, "Stability-centric design of a droop-mounted adaptive nonlinear control for EV charging in DC microgrid," 2024.
[15] Q. Xu, N. Vafamand, L. Chen, T. Dragicevic, L. Xie, and F. Blaabjerg, "Review on advanced control technologies for bidirectional DC/DC converters in DC microgrids," IEEE J. Emerg. Sel. Topics Power Electron., vol. 9, no. 2, pp. 1205–1221, Apr. 2021.
[16] S. J. Shern, M. T. Sarker, G. Ramasamy, S. P. Thiagarajah, F. Al Farid, and S. T. Suganthi, "Artificial intelligence-based electric vehicle smart charging system in Malaysia," 2024.
[17] Z. Wang, X. Lai, and Q. Wu, "A PSR CC/CV flyback converter with accurate CC control and optimized CV regulation strategy," IEEE Trans. Power Electron., vol. 32, no. 9, pp. 7045–7055, Sep. 2017.
[18] V.-L. Tran, H.-N. Vu, D.-D. Tran, and W. Choi, "Design and implementation of a high-efficiency multiple output charger based on the time-division multiple control technique," IEEE Trans. Power Electron., vol. 32, no. 2, pp. 1210–1219, Feb. 2017.
[19] H.-N. Vu and W. Choi, "A novel dual full-bridge LLC resonant converter for CC and CV charges of batteries for electric vehicles," IEEE Trans. Ind. Electron., vol. 65, no. 3, pp. 2212–2225, Mar. 2018.
[20] Z. Chen and X. Shu, "Optimal charging strategy design for lithium-ion batteries considering minimization of temperature rise and energy loss," May 2019.
[21] SHUCHANG WANG, YUSHEN LIU, AND XUEFENG WANG “Resonant Converter for Battery Charging Applications With CC/CV Output Profiles," 2020
[22] A. Bouscayrol, B. Davat, B. De Fornel, B. François, J. P. Hautier, F. Meibody-Tabar, and M.Pietrzak-David, Multimachine multiconverter system: application for electromechanical drives, EPJ Applied Physics, vol. 10, no. 2, 2000.
[23] A. Bouscayrol, X. Guilaud, J. Hautier, and P. Delarue, Macro modélisation des convertisseurs électromécaniques application à la commande des machines électriques, RIGE, vol. 2, no. 2, 2000.
[24] P. Delarue, A. Bouscayrol, A. Tounzi, X. Guillaud, and G. Lancigu, Modelling, control and simulation of an overall wind energy conversion system, vol. 28, no. 8, pp. 1169-1185, 2003
[25] L. Boulon, D. Hissel, A. Bouscayrol, and M.C. Pera, “From modeling to control of a PEM cell using Energetic Macroscopic Representation," Procee IEEE Transactions on Industrial Electronics, vol. 57, no. 6, pp. 1882-1891, 2010